

SPIN-CHARGE GAUGE SYMMETRY: A WAY TO TACKLE HTS CUPRATES?

P.A. Marchetti

Dipartimento di Fisica “G. Galilei”, INFN, I-35131 Padova, Italy

Z.B. Su and L. Yu

*Institute of Theoretical Physics and Interdisciplinary Center of Theoretical Studies,
Chinese Academy of Sciences, 100080 Beijing, China*

(Dated: September 9, 2018)

We propose an explanation of several experimental features of transport phenomena in the normal state of high T_c cuprates in terms of a spin-charge gauge theory of the 2D t - J model. The calculated doping (δ)-temperature (T) dependence for a number of physical quantities is found in qualitative agreement with data. In particular, we recover: in the “pseudogap phase” the metal-insulator crossover of the in-plane resistivity and of the NMR “relaxation time” (T_1T)⁶³ and the insulating behavior of the out-of-plane resistivity; in the “strange metal phase” (at higher T or δ) the linear in T behavior of the above quantities; the appearance of maxima in the in-plane far-infrared conductivity in strongly underdoped and overdoped samples.

PACS numbers: 71.10.Hf, 71.27.+a, 74.25.Fy, 74.25.Gz

THE SPIN-CHARGE GAUGE APPROACH

We assume as a model for CuO layers in high T_c cuprates the 2D t - J model. However, neglecting from beginning the n.n.n. hopping all features depending on the detailed structure of the Fermi surface are clearly lost. Gauging with a Chern-Simons gauge field action the spin and the charge global symmetries of the t - J model one obtains a gauged t - J model strictly equivalent to the original [1]. The spin-charge gauged model suggests an improved “Mean Field Approximation” (MFA) based on a formal spin-charge decomposition of the electron field [2]. In this approach, the low energy effective action describes spin 1/2 gapful bosonic spinons, with a non-linear sigma (NL σ) model action, and charged fermionic holons interacting via a slave-particle gauge field. Peculiar to our approach and present both in the “pseudogap” and “strange metal phases” (although here less effective) is the spinon gap $m_s \sim J(\delta |\ln \delta|)^{1/2}$. It is due to spin vortices attached by the spin gauge field in MFA to the empty-site positions and at high temperature it receives the standard thermal correction of the NL σ model. The theoretically derived $\delta - T$ dependence of the spinon gap up to $\sim 500K$ is in qualitative agreement with the behavior of the AF correlation length in underdoped LSCO [3].

In the “pseudogap phase” (PG, at low δ and T) the holons have “small” Fermi surface ($\epsilon_F \sim t\delta$) and a “Dirac structure” induced via Hofstadter mechanism by the π -flux lattice of the charge-gauge field in MFA, with bare dispersion

$$\epsilon^{PG}(\vec{p}) = \pm 2t \sqrt{\cos^2(p_x) + \cos^2(p_y)}$$

restricted to the magnetic Brillouin zone. The main effect of gauge fluctuations is to induce a shift in the mass of spinons [4] $m_s \rightarrow M = (m_s^2 - icT/\chi)^{1/2}$, where c

is a constant and χ the diamagnetic susceptibility, thus introducing a dissipation $\sim T$. The competition between the two energy scales, m_s^2 and T/χ , is the root in our approach of many crossover phenomena peculiar to in-plane transport properties of the “pseudogap phase” [5]. In particular it yields an explanation of the metal-insulator crossover (MIC) observed in underdoped, non-superconducting cuprates as temperature decreases [6], [7] and a similar crossover in superconducting cuprates when a strong magnetic field suppresses superconductivity [8]. Hence, in our approach the MIC is due to correlation effects, not to a disorder-induced localization which would be hard to reconcile with the experimental fact that $k_F\ell$ at MIC ranges from O(0.1) to O(10), i.e. well below and well above Ioffe-Regel limit. Furthermore the gauge interaction induces the binding of spinon and anti-spinon into a massive damped magnon resonance and (close to the Fermi surface) of spinon and holon into an “electron” resonance with a $T^{1/6}$ -dependent wave function renormalization constant Z and inverse life-time $\Gamma \sim |M| \sin \arg(M)$. This energy scale, i.e. the recombination rate, dominates the out-of-plane resistivity, yielding an insulating behavior. The “Dirac dispersion” of holons induces a reduction of the spectral weight outside the magnetic Brillouin zone, reminiscent of the “Fermi arcs” found in ARPES in underdoped cuprates [9], see Fig.1.

Around a temperature T^* (identifiable as the inflection point of in-plane resistivity) the π -flux lattice of the charge gauge field melts and we enter in the “strange metal phase” (SM, at high δ or T). In such phase [10], holons have “large” Fermi surface ($\epsilon_F \sim t(1 - \delta)$) and standard dispersion. The gauge fluctuations induce still the formation of a strongly overdamped magnon resonance, with inverse life-time $\sim TQ_0/(\chi m_s^2) \sim T^{4/3}$ and an “electron resonance” with inverse life-time Γ , of

the same order and $Z \sim \sqrt{m_s Q_0}/J \sim T^{1/6}$. $Q_0^{-1} = (\chi/\kappa T)^{1/3}$ is the typical scale of gauge fluctuations, where κ is their Landau damping, and can be thought of as a sort of anomalous skin depth. Consistently with experimental data, linear in T behaviour of in-plane and out-of-plane resistivity and spin relaxation time $(TT_1)^{63}$ is recovered at large enough T , as a consequence of the above life-time and the “effectiveness” of the gauge fluctuations in a slab of momenta $Q_0 \sim T^{1/3}$ around the Fermi surface: in fact the conductivity derived from Boltzmann transport theory would be $\sigma_0 \sim \Gamma^{-1}$, but due to “effectiveness” the physical conductivity is $\sigma \sim \sigma_0 Q_0 \sim T^{-4/3} T^{1/3} \sim T^{-1}$.

BEHAVIOR OF PHYSICAL QUANTITIES

In-plane resistivity

It is calculated via Ioffe-Larkin addition rule [11], a typical feature of slave-particle gauge theories: $\rho = \rho_s + \rho_h$, where ρ_s is the resistivity of the spinon-gauge subsystem and ρ_h of the holon-gauge subsystem, subdominant. Kubo formula applied to ρ_s gives in the PG in the range $m_s Q_0 \lesssim T/\chi \lesssim m_s^2$ (roughly from few tenth to few hundreds K) where the approximations made appear reliable,

$$\rho \sim \rho_s \sim \frac{|M|^{1/2}}{\sin(\arg \frac{M}{2})} \sim \begin{cases} T^{-1} & m_s^2 \gg \frac{cT}{\chi} \\ \sim T^{-\frac{1}{4}} & m_s^2 \sim \frac{cT}{\chi} \end{cases} \quad (1)$$

Thus one recovers the metal-insulator-crossover (MIC) and an inflection point $T^* \sim \chi m_s^2 \sim |\ln \delta|$ (since $\chi \sim \delta^{-1}$ in PG) at higher temperature, found also experimentally [6]; see Fig. 2. One easily verifies that the normalized resistivity $\rho_n = (\rho - \rho(T_{MIC})) / (\rho(T^*) - \rho(T_{MIC}))$ is a function only of the ratio $T/(\chi m_s^2)$. Therefore a prediction of the theory is a universal behaviour which in fact can be verified in experimental data and was already empirically remarked in [7], [12]. See Fig. 3,4. The introduction of a magnetic field perpendicular to the plane yields a shift of the MIC at higher temperature and this in turn produces a big positive transverse magnetoresistance [13], as found in experiments [14].

In SM one obtains, for $m_s, \Gamma \lesssim Q_0$ (roughly from few tenth to 500 K), where the approximation made in our approach are reasonable:

$$\rho_s \simeq 2\lambda Q_0^{-1}(\Gamma + m_s^2/\Gamma) = \frac{T}{\chi m_s^2} \lambda^2 + \frac{32m_s^4 \chi}{T Q_0^2}, \quad (2)$$

where $\lambda \sim O(1)$ is a constant. In the high temperature limit $Q_0 \gg m_s$, the damping rate in (2) dominates over the spin gap $2m_s$ and the spinon contribution to resistivity is linear in T , with a slope $\alpha \simeq (1 - \delta)/(\delta |\ln \delta|)$, see Fig. 5. Lowering the temperature, the second term in (2) gives rise first to a superlinear behavior and then, at the

margin of validity of our approach, an unphysical upturn. The deviation from linearity is due to the spin gap effects and is cutoff in the underdoped samples by the crossover to the PG phase. We expect that physically in the overdoped samples it is cutoff by a crossover to a FL “phase”. The temperature dependence of the spinon mass yields a bending at high temperature, stronger for lower dopings, as visible in the resistivity data at constant volume for LSCO [15]; this effect is masked in the resistivity data at constant pressure [6] by thermal expansion.

In-plane IR electronic AC conductivity

We compute the electronic AC conductivity via Kubo formula, in the two limits $\Omega \ll T$, $T \ll \Omega$, where Ω is the external frequency. It turns out that up to the logarithmic accuracy one can pass from the first to the second limit by replacing T with Ω in Q_0 and Γ (we denote the obtained quantities by Q_Ω, Γ_Ω) and rescaling Γ by a positive multiplicative factor $\lambda \lesssim 1/2$. In PG, in the range $T \lesssim \Omega \lesssim Jm_s^2$ the AC conductivity can be approximately obtained from ρ^{-1} derived from eq. (1) substituting T with $\tilde{\lambda}\Omega$. Hence it exhibits a broad maximum at a frequency, Ω_{MIC} , corresponding to a temperature slightly higher than T_{MIC} , as in fact experimentally seen in [16], see Fig. 6, 7. An $a - b$ anisotropy of T_{MIC} and Ω_{MIC} found in underdoped LSCO [16] would be generated naturally in the above scheme by an $a - b$ anisotropy of the magnetic correlation length [17]. The anisotropy of T_{MIC} strengthens our interpretation of correlation-induced MIC, since a disorder-induced localization is expected to have a unique MIC temperature. As T becomes greater than Ω the AC conductivity becomes approximately Ω independent.

In SM, for $\Omega \ll T$ we have

$$\sigma(\Omega, T) \sim \frac{Q_0}{i(\Omega - 2m_s) + \Gamma} \sim \frac{1}{i(\Omega - 2m_s)T^{-1/3} + T}, \quad (3)$$

while for $T \ll \Omega$

$$\sigma(\Omega, T) \sim \frac{Q_\Omega}{i(\Omega - 2m_s) + \tilde{\lambda}\Gamma_\Omega} \sim \frac{1}{i(\Omega - 2m_s)\Omega^{-1/3} + \Omega}. \quad (4)$$

From the above formulas the following features found experimentally in overdoped LSCO [18] and BSCO [19] are easily derived: besides the standard tail $\sim \Omega^{-1}$, the effect of replacing Q_0 by Q_Ω is to asymmetricize the peak at $2m_s$ appearing in $\text{Re}\sigma(\Omega, T)$ for $\Omega \ll T$ and to shift it towards lower frequency, see Fig. 8.

Spin-lattice relaxation rate $(1/T_1 T)^{63}$

It is calculated via Kubo formula. In the PG one finds:

$$\left(\frac{1}{T_1 T}\right)^{63} \sim (1 - \delta)^2 |M|^{-\frac{1}{2}} \left(a \cos\left(\frac{\arg M}{2}\right) + b \sin\left(\frac{\arg M}{2}\right) \right) \sim \begin{cases} T & m_s^2 \gg \frac{cT}{\chi} \\ \sim T^{-\frac{1}{4}} & m_s^2 \sim \frac{cT}{\chi} \end{cases} \quad (5)$$

Therefore we obtain a broad peak as observed in some

cuprate [20], see Fig 9. In SM one finds

$$\left(\frac{1}{T_1 T}\right)^{63} \sim (1 - \delta)^2 \rho_s^{-1}. \quad (6)$$

Therefore, in the high temperature limit we recover the linear in T behavior for $(T_1 T)^{63}$ and at high doping / low temperature the superlinear deviation, also found experimentally in overdoped samples of LSCO.[21], see Fig. 10. Furthermore, the factor $(1 - \delta)^{-2}$ weakens the doping dependence of the slope as compared with the resistivity curves, in agreement with the experimental data.

Out-of-plane resistivity

We assume an incoherent transport along c -direction. ρ_c thus is dominated by virtual hopping between layers and it is calculated via Kumar- Jayannavar formula [22]:

$$\rho_c \sim \frac{1}{\nu} \left(\frac{1}{\Gamma} + \frac{\Gamma}{t_c^2 Z^2} \right), \quad (7)$$

where Γ is the inverse electron life time, given here by the spinon-holon recombination rate, t_c is an effective average hopping in the c -direction and ν the density of states at the Fermi energy. In PG the first term in (7) dominates, yielding the insulating behaviour:

$$\rho_c \sim (|M| \sin(\arg M))^{-1} \sim \begin{cases} T^{-1} & m_s^2 \gg \frac{cT}{\chi} \\ \sim T^{-\frac{1}{2}} & m_s^2 \sim \frac{cT}{\chi} \end{cases}$$

. This crossover reproduces a knee experimentally found in [23], see Fig. 11. The very strong decrease with T of the anisotropy ratio $\rho_c(T)/\rho_{ab}(T)$ in PG is also well reproduced by the above formulas, see Fig. 12.

In the SM phase the second, metallic, term in (7) dominates and substituting Γ and Z one recovers the T -linearity in the ‘‘incoherent regime’’ $\Gamma \gg t_c Z$:

$$\rho_c \simeq \frac{J^2}{t_c^2 m_s \nu} \frac{T}{\chi m_s^2} \simeq \frac{T}{(\delta |\ln \delta|)^{3/2}}. \quad (8)$$

The second term in eq. (7) yields possibly a minimum at low T (if in the admissible range) see Fig. 13. Unfortunately, we don’t have a reliable method to estimate the (extrapolated) $T = 0$ intercept of $\rho_c(T)$ which is large when compared with the corresponding intercept for ab -plane resistivity, so we cannot extract safely the anisotropy ratio $\rho_c(T)/\rho_{ab}(T)$. However, if the minimum in ρ_c is at higher temperature than the (unphysical) minimum in ρ_{ab} , then one can derive the fast decrease of the anisotropy ratio at low temperature found experimentally,[24] , see Fig. 14.

We would like to sincerely thank J.H. Dai, L. De Leo and G. Orso for their collaboration at different stages of this project.

-
- [1] J. Fröhlich and P.A. Marchetti, Phys. Rev. B **46**, 6535 (1992).
 - [2] P.A. Marchetti, Z.B. Su, L. Yu, Phys. Rev. B **58**, 5808 (1998).
 - [3] B. Keimer *et al.*, Phys. Rev. B **46**, 14034 (1992).
 - [4] P.A. Marchetti, J.H. Dai, Z.B. Su and L.Yu, J. Phys. Condens. Matt. **12**, L329 (2000).
 - [5] P.A. Marchetti, L. De Leo, G.Orso, Z.B. Su and Yu Lu, Phys. Rev. B **69** 024527 (2004).
 - [6] H. Takagi *et al.*, Phys. Rev. Lett. **69** (1992) 2975.
 - [7] B. Wuyts *et al.*, Phys. Rev. **B53** (1996) 9418.
 - [8] P. Fournier *et al.*, Phys. Rev. Lett. **81** (1998) 4720; S. Ono *et al.*, Phys. Rev. Lett. **85** (2000) 638; K. Segasawa and Y. Ando, Phys. Rev. **B59** (1999) R 3948; Y. Ando *et al.*, Phys. Rev. Lett. **75** (1995) 4662; G.S. Boebinger *et al.*, Phys. Rev. Lett. **77**(1996) 5417; Y. Ando *et al.* J. Low Temp. Phys. **(105)** (1996) 867
 - [9] A. Damascelli, Z. Hussain, and Z.X. Shen, Rev. Mod. Phys. **75**, 473 (2003).
 - [10] P.A. Marchetti, G.Orso, Z.B. Su and Yu Lu, Phys. Rev. B **71**, 134510 (2005).
 - [11] L. Ioffe and A. Larkin, Phys. Rev. B **39**, 8988 (1989).
 - [12] Z. Konstantinovic *et al.*, Physica C **341**, 859 (2000).
 - [13] P.A. Marchetti, Z.B. Su and L. Yu, Phys. Rev. Lett. **86**, 3831 (2001).
 - [14] A. Lacerda *et al.*, Phys. Rev. B **49**, 9097 (1994); T. Kimura *et al.*, Phys. Rev. B **53**, 8733 (1996); Y. Abe *et al.*, Phys. Rev. B **59**, 14753 (1999).
 - [15] B. Sundqvist and E.M.C. Nilsson, Phys. Rev. B **51**, 6111 (1995); K. Takenaka *et al.*, Phys. Rev. B **68**, 134501 (2003).
 - [16] M. Dumm, D. N. Basov, S. Komiyama, and Y. Ando, Phys. Rev. Lett. **91**, 077004 (2003).
 - [17] P.A. Marchetti, G. Orso, Z.B. Su and L. Yu, Phys. Rev. B **69**, 214514 (2004).
 - [18] T. Startseva *et al.*, Physica C **321**, 135 (1999).
 - [19] S. Lupi *et al.*, Phys. Rev. B **62**, 12418 (2000).
 - [20] C. Berthier *et al.*, Physica C **235-240**, 67 (1994).
 - [21] C. Berthier *et al.*, J. Physique I **6**, 2205 (1997); S. Fujiiyama *et al.*, J. Phys. Soc. Jpn. **66**, 2864 (1997).
 - [22] N. Kumar and A.M. Jayannavar, Phys. Rev. B **45**, 5001 (1992); N. Kumar *et al.*, Mod. Phys. Lett. B **11**, 347 (1997); Phys. Rev. B **57**, 13399 (1998).
 - [23] T.Ito *et al.*, Nature (London) **350** (1991) 596; Y.F. Yan *et al.*, Phys. Rev. B **52**, R751 (1995).
 - [24] Y. Nakamura and S. Uchida, Phys. Rev. B **47**, 8369 (1993).
 - [25] S. Komiyama *et al.* Phys. Rev. B **65**, 214535 (2002).
 - [26] T. Kimura *et al.*, Phys. Rev. B **53**, 8733 (1996); Y. Abe *et al.*, Phys. Rev. B **59**, 14753 (1999).

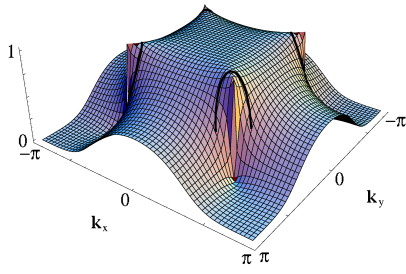


FIG. 1: Angle-dependent spectral weight of the electron propagator. The thick lines close to $(\pm\pi/2, \pm\pi/2)$ represent the region of FS with spectral weight larger than $1/2$ for $\delta \sim 0.05$

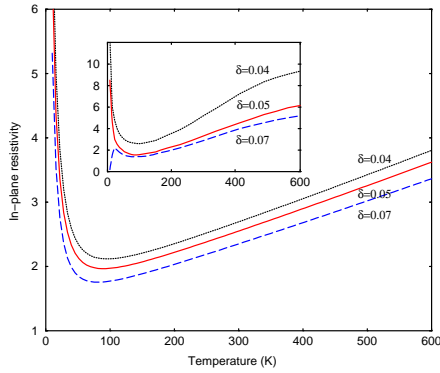


FIG. 2: The calculated temperature dependence of in-plane resistivity for various dopings δ in comparison with the corresponding experimental data (inset) on $\text{La}_{2-\delta}\text{Sr}_\delta\text{CuO}_4$ in units of $m\Omega\text{cm}$, taken from Ref. 6.

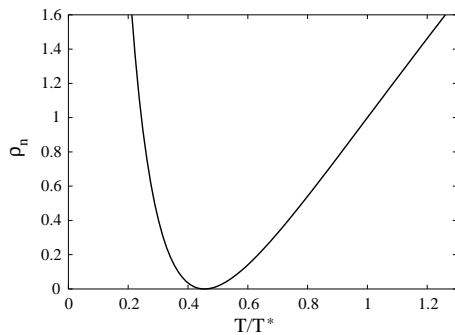


FIG. 3: Calculated “normalised” resistivity ρ_n versus reduced temperature T/T^* (see text for explanation).

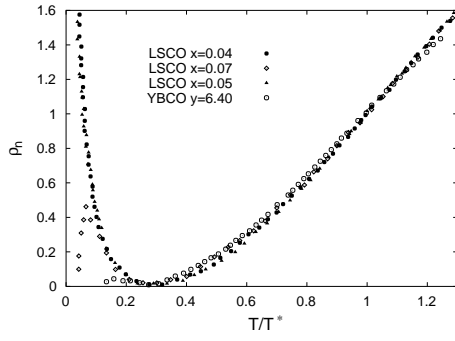


FIG. 4: Temperature dependence for ρ_n in underdoped LSCO (Extracted from Ref. 6) and YBCO (Extracted from Ref. 7)

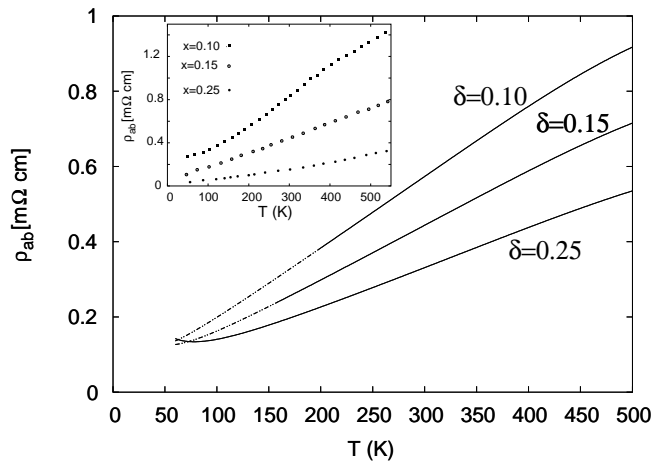


FIG. 5: Calculated in-plane resistivity as a function of temperature for different hole concentrations. Below the pseudogap temperature T^* , the curve is shown in dashed line. *Inset*: In-plane resistivity versus T measured in LSCO crystals with different Sr content x , taken from the work of Takenaka *et al.*, Ref. 15

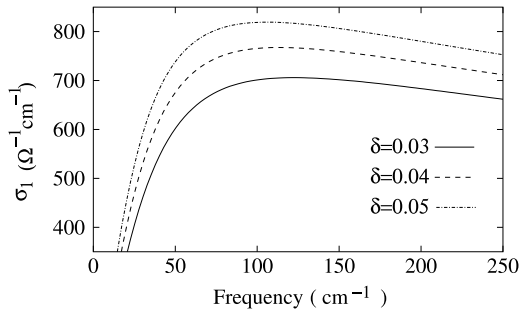


FIG. 6: Theoretically calculated frequency dependence of the AC conductivity for different dopings: $\delta = 0.03$ (full line), $\delta = 0.04$ (dashed) and $\delta = 0.05$ (dotted).

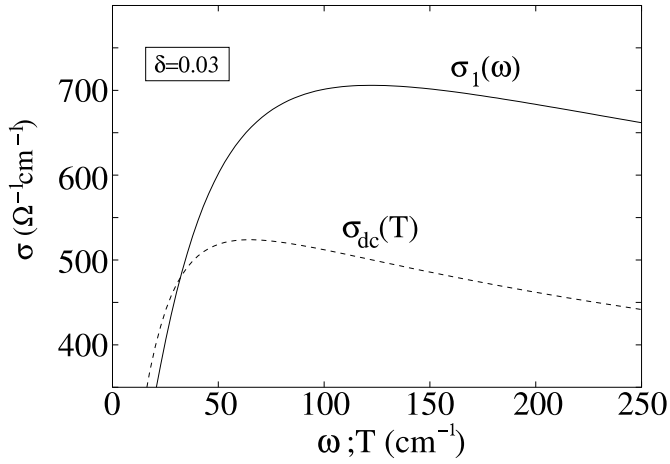


FIG. 7: Calculated frequency dependence of the AC conductivity for $\delta = 0.03$. Also shown is the corresponding DC conductivity as a function of temperature (in cm^{-1}).

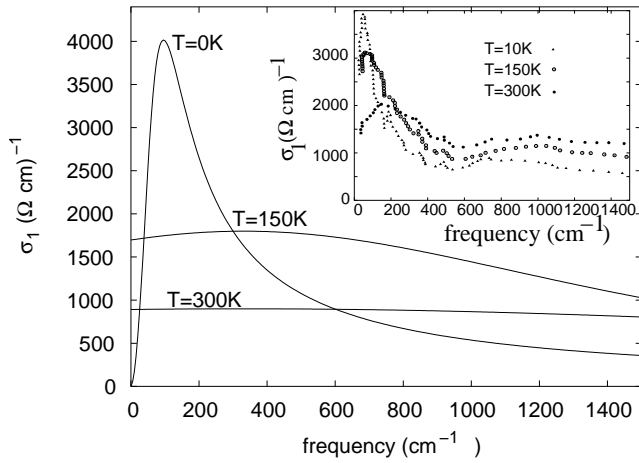


FIG. 8: Calculated AC conductivity as a function of frequency for fixed hole density $\delta = 0.184$ and different temperatures. *Inset*: AC conductivity versus frequency measured for a LSCO sample with $x = 0.184$ at different temperatures, taken from the work of Startseva *et al.*, Ref. 18.

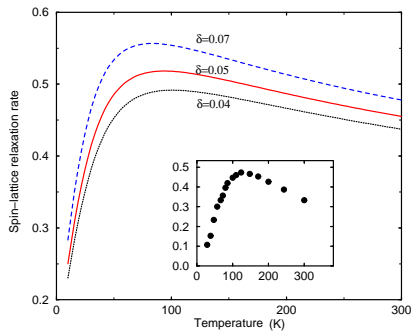


FIG. 9: The calculated temperature dependence of spin-lattice relaxation rate $(1/T_1T)^{63}$ for different dopings. *Inset* data of $\text{YBa}_2\text{Cu}_3\text{O}_{6.52}$ single crystal in units of $s^{-1}K^{-1}$, taken from Ref. 20.

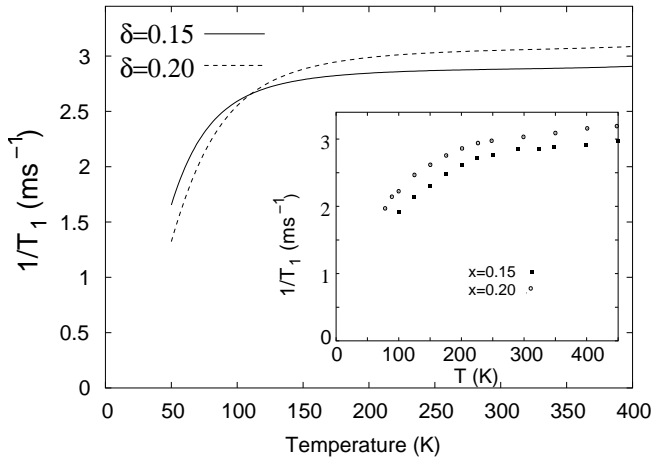


FIG. 10: Calculated temperature dependence of the spin-lattice relaxation rate $1/T_1$ for different doping concentrations. *Inset*: spin-lattice relaxation rate measured in LSCO samples with different Sr content x , taken from the work of Fujiyama *et al.*, Ref. 21.

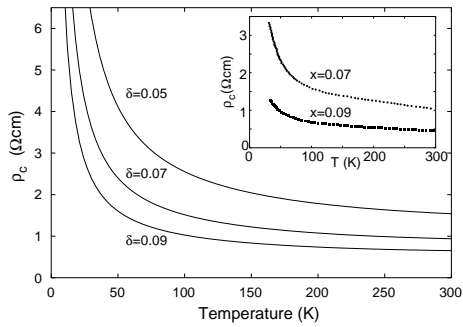


FIG. 11: Calculated temperature dependence of the out-of-plane resistivity (in arbitrary units) for different doping concentrations: $\delta=0.05$ (full line), $\delta=0.07$ (dashed) and $\delta=0.09$ (dotted). Inset shows experimental data on LSCO, extracted from Ref. 26

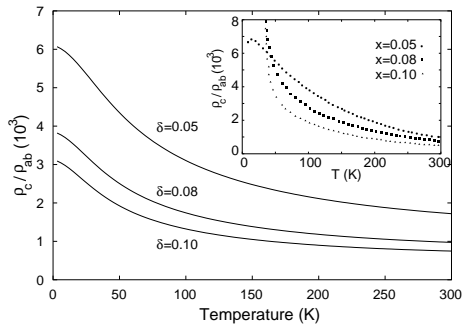


FIG. 12: Calculated temperature dependence of the resistivity anisotropy ratio as a function of temperature for different doping concentration: $\delta=0.05$ (full line), $\delta=0.07$ (dashed) and $\delta=0.09$ (dotted). Inset shows corresponding experimental data on LSCO, extracted from Ref. 25

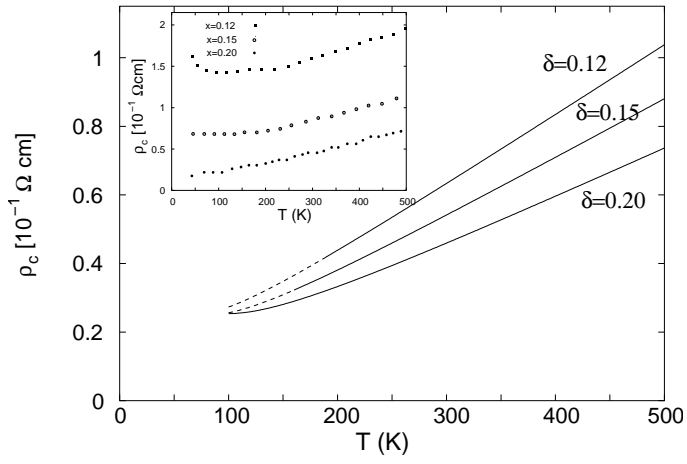


FIG. 13: Calculated out-of-plane resistivity as a function of temperature for different hole concentrations. Below the pseudo-gap temperature T^* , the curve is shown in dashed line. *Inset*: In-plane resistivity versus T measured in LSCO crystals with different Sr content x , taken from the work of Nakamura *et al.*, Ref. 24

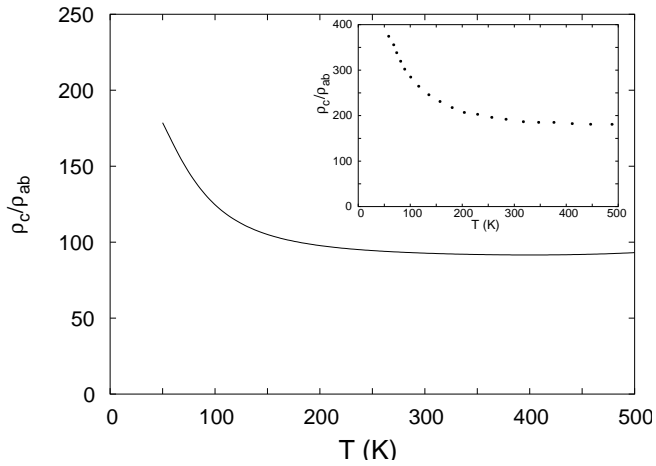


FIG. 14: Calculated resistivity anisotropy ratio as a function of temperature for fixed hole density $\delta = 0.2$. *Inset*: resistivity anisotropy ratio measured for a LSCO sample with Sr content $x = 0.20$, taken from the work of Nakamura *et al.*, Ref. 24.